**Running head: A CLOCK OVERHAUL FOR POPULATION GENETICS**

# Late-Glacial Demographic Expansion Motivates a Clock Overhaul for Population Genetics

Thierry B Hoareau[a]

[a]*Molecular Ecology and Evolution Programme, Department of Genetics, University of Pretoria, Private bag X20, Hatfield, Pretoria 0028, South Africa. E-mail: thoareau@gmail.com, Tel. +27 12 420 3871 Fax. +27 12 362 5327*

Correspondence should be addressed to Thierry B Hoareau at the above postal or email address

*Abstract*.–The molecular clock hypothesis is fundamental in evolutionary biology as by assuming constancy of the molecular rate it provides a time frame for evolution. However, increasing evidence shows time dependence of inferred molecular rates with inflated values obtained using recent calibrations. As recent demographic calibrations are virtually non-existent in most species, older phylogenetic calibration points (>1 Ma) are commonly used, which overestimate demographic parameters. To obtain more reliable rates of molecular evolution for population studies, I propose the Calibration of Demographic Transition (CDT) method, which uses the timing of climatic changes over the late glacial warming period to calibrate expansions in various species. Simulation approaches and empirical datasets from a diversity of species (from mollusk to humans) confirm that, when compared to other genealogy-based calibration methods, the CDT provides a robust and broadly applicable clock for population genetics. The resulting CDT rates of molecular evolution also confirm rate heterogeneity over time and among taxa. Comparisons of expansion dates with ecological evidence confirm the inaccuracy of phylogenetically derived divergence rates when dating population-level events. The CDT method opens opportunities for addressing issues such as demographic responses to past climate change and the origin of rate heterogeneity related to taxa, genes, time and genetic information content.

**Key words:** Bayesian Skyline Plots, Calibration of Demographic Transition, Expansion Dating, Molecular Calibration, Molecular Rate, Two-Epoch Model, Time Dependency

The molecular clock hypothesis, which suggests that evolution occurs at a constant rate over time, was first proposed over fifty years ago (Zuckerkandl and Pauling 1962) and has proven invaluable for establishing a timeline for evolutionary change (Kumar 2005). The neutral and nearly neutral theories of evolution (Kimura 1968; Ohta 1973) support this hypothesis by providing a solid framework predicting clock-like mutation. Nevertheless, the notion of a constant molecular rate implied by the molecular clock is contradicted by mounting evidence supporting rate heterogeneity among taxa (Kumar 2005; Baer et al. 2007; Bromham 2011).

There is growing evidence that inferred molecular rates may have inflated values that converge towards instantaneous rates when derived from more recent calibration dates (Ho et al. 2011a for a review). The relationship between the molecular rate and calibration date was previously described (Ho et al. 2005; Ho and Larson 2006), and has subsequently been verified for various genes and taxa (Howell et al. 2007; Ho et al. 2007; Burridge et al. 2008; Papadopoulou et al. 2010; Crandall et al. 2012; Duchene et al. 2014). Moreover, standard models of population genetics predict this apparent acceleration of the rates estimated over recent timescales, when accounting for ancestral polymorphism (Peterson and Masel 2009). According to this model, the "demographic rate" obtained from modern calibrations (pedigree and ancient DNA or aDNA) is significantly higher than the widely accepted 1% "phylogenetic molecular rate" (0.01 changes/site/myr), which is often obtained when using divergence calibrations (e.g. paleontological data or biogeographic events) for mtDNA protein-coding genes within vertebrate lineages (Brown et al. 1979; Shields and Wilson 1987; Fleischer et al. 1998).

Apart from a few species such as humans (e.g. Brotherton, Haak et al. 2013; Fu et al. 2013), Beringian megafauna (e.g. Lorenzen et al. 2011) or Antarctic fauna (e.g. Millar et al. 2008), for which pedigree data and/or aDNA are available, most population studies lack

modern calibrations and rely on phylogenetic calibrations derived from biogeographic events (e.g. Lessios 2008) or paleontological data (fossils; Laurin 2012). If the time dependency of inferred molecular rate is confirmed across a wide range of taxa and genes, consistent overestimation of demographic and evolutionary parameters can be expected. These parameters include effective population size (*Ne*), gene flow and divergence time (Ho et al. 2008), which are central to conservation genetics (Ho and Larson 2006). Alternative rates, derived from relatively recent calibration points, would probably provide more accurate estimates of evolutionary processes at the population scale.

Alternative methods have recently been developed to overcome the biases of using phylogenetic calibrations to estimate population parameters. These include the use of recent geological or historical events to calibrate population divergences (Burridge et al. 2008; Papadopoulou et al. 2010), or time to the most recent common ancestor (*TMRCA*) of a specific lineage (Ho and Endicott 2008; Henn et al. 2009; Herman and Searle 2011). Other researchers have used multi-demographic coalescent models to account for variance of evolutionary rates across genealogies and among lineages (Ho et al. 2008; Marino et al. 2011). Demographic expansions have also been calibrated based on late Pleistocene postglacial climate change (Ruzzante et al. 2008; Crandall et al. 2012; Grant and Cheng 2012; Grant et al. 2012).

Expansion dating (Crandall et al. 2012) is a promising approach which assumes that the late glacial rise in sea level increased habitat availability, causing demographic expansion in three tropical marine invertebrates. Crandall et al. (2012) used a two-epoch coalescent model to recover coalescent events coinciding with the demographic transition (Shapiro et al. 2004). These were calibrated by prior dating of the initial late glacial increase in habitats (19.6 and 14.6 ka). The increased rates inferred by this study demonstrate the importance of using environmental histories as independent proxies to calibrate demographic events. This

promising approach opens opportunities for calibration in species that lack accurate molecular rates, but the focus on the shallow-water habitats on the Sunda Shelf limits its application. Nevertheless, alternate demographic proxies could broaden its utility.

The association between climatic cycles and fluctuations in population size is widely recognized in a broad range of environments (Rodriguez-Banderas et al. 2009; Hoareau et al. 2012; Bagley et al. 2013). As such, it represents a framework to estimate recent rates of molecular evolution for many organisms. Although some temperate and Arctic species experience a simple range shift (e.g. Prost et al. 2013) and others an expansion associated with the glacial period (e.g. Rambaut et al. 2009; Lorenzen et al. 2011), most species follow a glacial contraction/post-glacial expansion model. During glacial periods, these species retreat into refugia and experience genetic bottlenecks, followed by demographic and range expansions associated with habitat release during postglacial warming (Hewitt 2000; Provan and Bennett 2008; Fraser et al. 2012). For species fitting this model, a correlation is assumed to exist between temperature change and population growth during the postglacial period. Under these assumptions, temperature can be used as a demographic proxy for calibration of the species genealogy (Rajabi-Maham et al. 2008; Grant and Cheng 2012; Grant et al. 2012).

In order to broaden the applicability of the expansion dating method, I explore the utility of temperature as a proxy for historical population size changes. I address some challenges presented by the method, by selecting organisms matching the contraction-expansion model. Also, I incorporate the full distribution of calendar times corresponding to the increase in temperature between 10 and 20 ka, instead of using a single calibration date as applied by Crandall et al. (2012). This conceptual framework provides a robust method for the calibration of demographic transition (CDT method).

Here, I evaluate the utility of this method based on simulations and empirical data from multiple species (terrestrial and aquatic, tropical and temperate). Validation is performed using simulated data mirroring a demographic expansion that coincides with the recent postglacial warming. Application of the method to various species affected by the postglacial warming gives estimates of molecular evolutionary rates (hereinafter referred to as the CDT rate). These results are then used to explore rate heterogeneity among taxa and over time. Finally, I investigate the reliability of the CDT and alternative calibration methods by both comparing the match between the timing of expansions and the expectations of ecological changes (Holocene, glacial period and previous interglacial) and assessing the reliability of the rate estimates for each period.

## MATERIAL AND METHODS

### *Datasets*

One hundred non-recombining gene sequence datasets were simulated using inferred temperature variation between 20 and 10 ka as a proxy for changes in *Ne* (online Appendix 1). The rapid cooling of the climate in the Northern Hemisphere associated with the Younger Dryas (12.9–11.7 ka; Bakke et al. 2009) was included, to simulate a hiatus in population growth that interrupted the expansion. Ancestral and modern *Ne* were set to $10^4$ and $10^6$ respectively, which matches realistic demographic changes (Ho and Endicott 2008). Each simulated data set included 100 sequences of 500 nucleotides for five mtDNA segments (2500 bp when combined), and were obtained using the program DIYABC v1.0.4.46 (Cornuet et al. 2010). The five genes were simulated separately and then concatenated for further analyses. The mutation rate was set to 0.3 changes/site/myr (HKY substitution model), which corresponds to rates obtained from aDNA studies (e.g. Ho et al. 2011b). To

assess the effect of genetic resolution, these complete datasets were complemented by reduced datasets of 100 sequences of only 500 nucleotides.

Temperate species from a range of taxa and environments were chosen from the literature (Table 1; details in Appendix 1), based on the expectations of a demographic expansion (i.e. logistic growth model), occurring during the transition period between the Last Glacial Maximum (LGM; 20 ka) and the Holocene (11.7 ka). Selected species included the rough periwinkle (*Littorina saxatilis*; Panova et al. 2011), bark beetle (*Pityogenes chalcographus*; Bertheau et al. 2013), chocolate chip starfish (*Protoreaster nodosus*; Crandall et al. 2012), stickleback (*Gasterosteus aculeatus*; Mäkinen and Merilä 2008), Chiloe Island ground frog (*Eupsophus calcaratus*; Nuñez et al. 2011), brown bear (*Ursus arctos*; Korsten et al. 2009) and human (*Homo sapiens sapiens*; Li et al. 2014). The starfish is a tropical species, but was also included based on evidence of an expansion over the same period (Crandall et al. 2012).

*Demographic Analyses*

Figure 1 provides an overview of the procedure implemented in the CDT method. After selecting datasets (Fig. 1a), the program MAFFT v6 online (http://mafft.cbrc.jp/alignment/server/) was used to align the sequence data (Fig. 1b). Substitution models were selected based on Akaike Information Criterion values calculated in MEGA v5.01 (Tamura et al. 2011).

For each dataset, the demographic history was reconstructed using Bayesian Skyline models (BSPs; Fig. 1c; Drummond et al. 2005). The BSP model is a coalescent method sampling genealogies and parameters using a Markov chain Monte Carlo (MCMC) approach available in BEAST v1.7.1 (Drummond and Rambaut 2007). It is a versatile model as it allows for reconstruction of *Ne* through time, without imposing any specific constraints on

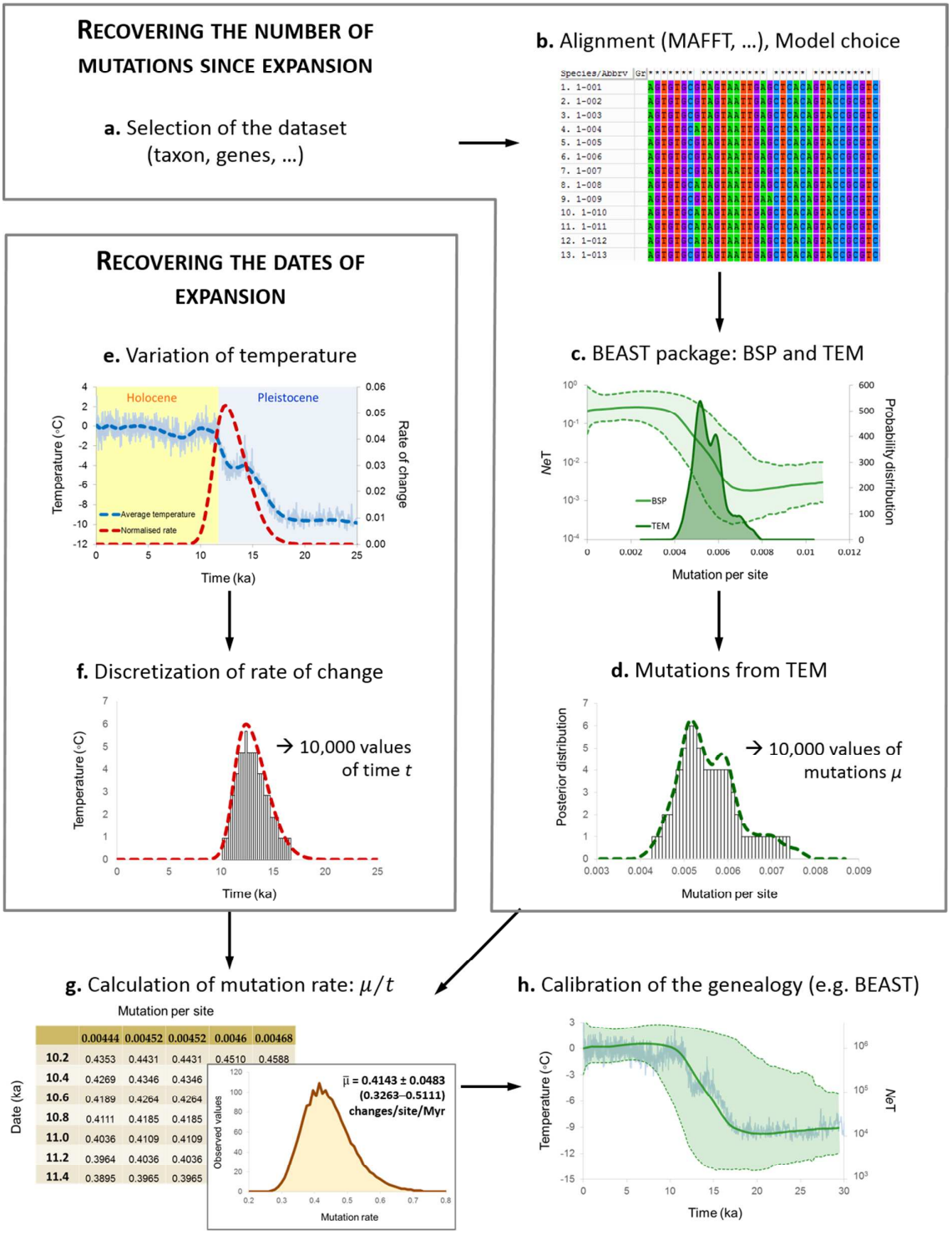


**Figure 1.** Overview of the procedure implemented in the CDT method. After the selection of the datasets (**a**), the sequences are aligned and the best model of molecular evolution is selected (**b**). Using the package BEAST, the BSP and TEM are reconstructed (**c**) and the TEM provides 10,000 values of mutation per site (since the demographic transition). The rate of change of the temperature over the last 25 kyrs is calculated (**e**) and the curve is discretized to obtain 10,000 values of calendar dates (**f**). Both mutation and date values are used to calculate $10^8$ values of the mutation rate (**g**). The mean and standard deviation of the mutation rate are used to calibrate the genealogy (**h**).

the demographic model. The molecular clock was not calibrated. The MCMC chains were run from 22 to 330 million iterations to recover 10,000 genealogies and model parameters, after discarding 10% of the samples as burn-in. The number of groups of coalescent intervals was set to ten and convergence was checked using the BEAST guidelines (effective sample size, ESS, above 200). Three independent runs were then combined and resampled to obtain the final 10,000 genealogies and associated parameter estimates. Changes in $NeT$ (with $T$ = generation time) were reconstructed from this genealogical sample using TRACER v1.5 (Drummond and Rambaut 2007).

The two-epoch coalescent model (TEM; Shapiro et al. 2004) of logistic population growth (available in BEAST), was used to recover the distribution of coalescent events coinciding with expansions (Fig. 1d; Crandall et al. 2012). This model estimates *Ne* in both the present ($N_0$) and in the past ($N_1$), as well as the transition time ($t_t$) between two epochs, each characterised by specific exponential population growth rates ($r_0$ and $r_1$). If time is not calibrated, the $t_t$ parameter represents the rate of changes per site accumulated in the genealogy since the time of demographic transition, which approximates the mutational time of the expansion. Molecular evolutionary models, sampling schemes and other settings were identical to those used for the BSPs, and the clock was not calibrated.

For all datasets, the best molecular clock model within the Bayesian Skyline framework was identified by comparing the strict clock with the uncorrelated relaxed clock with a lognormal distribution. Using the best-fit clock model, the logistic growth (population growth following and preceding a period of stable *Ne*) was verified for each empirical data set by comparing demographic models (constant population size and TEM). The selection of these models was explored over 1000 bootstrap replicates using a new marginal likelihood estimator available in TRACER v.1.6 (Rambaut et al. 2013). This estimator is based on a posterior simulation-based analogue of Akaike's information criterion using a Markov chain

Monte Carlo sampling algorithm (Baele et al. 2012), which outperforms the method based on harmonic mean estimation (Suchard et al. 2001).

New BSPs were then implemented for the simulated and empirical datasets (Fig. 1h), applying the best-fit clock model and several molecular rates (see following section). The above mentioned procedures were followed for the sampling scheme and to evaluate convergence. For all the datasets and molecular rates, the evolution of *NeT* was overlaid on the variation of temperature over the last 30 kyrs for the simulated datasets, and last 200 kyrs for the empirical datasets (see details below).

*Environmental Proxies and Molecular Rate Estimates*

To calibrate the expansions for both the simulated and empirical datasets, the variation of temperature (last 25 kyrs) was used as a demographic proxy (Fig. 1e-f), as expected under the contraction-expansion model. The temperature estimates were derived from deuterium measurements obtained from the Antarctic EPICA Dome C Ice Core (Jouzel et al. 2007; http://doi.pangaea.de/10.1594/PANGAEA.683655?format=html). A simple rectangular smoothing algorithm (smooth width = 51) was applied to the data. The rate of change was then calculated using the equation [$RC = (T_{n+1} - T_n)/(t_{n+1} - t_n)$] (with *T*: temperature and *t*: time), and the same rectangular smoothing algorithm (smooth width = 51) was applied to the rate of change (RC) values.

When plotted over time, the *RC* values gave a density curve (Fig. 1f) that was discretized to obtain 10,000 values of deuterium dates (*t*). These were then used to calibrate mutational time. The 95% Highest Posterior Density (HPD) of the TEM generated by BEAST, represented 10,000 values of mutation per site ($\mu$; Fig. 1d). These values of $\mu$ and *t* were used to build a matrix and calculate $10^8$ estimates of the CDT rate, using the equation $\mu/t$ (Fig. 1g). To implement this method, a script in R was written to calculate the average

CDT rate, as well as the standard deviation and the inner 95$^{th}$ percentile range. The script is available in online Appendix 2, and an example is available from the Dryad Digital Repository (doi:10.5061/dryad.7c65g). This script was used to calculate all molecular rates for both simulated and empirical datasets.

For the simulated datasets, two additional calibration methods were applied. The first procedure is the Calibration from Start of the Expansion and is referred to as the CSE rate. It calibrates the TEM, assuming that the start of the expansion coincides with the beginning of the postglacial warming period (19.6 ka; Crandall et al. 2012). The second is the Calibration of Population Coalescence time (CPC rate), as described by Endicott and Ho (2008), assuming synchrony of time to common ancestry (*TMRCA*) and the LGM (20 ka). For the empirical datasets, several additional molecular rates are compared. Phylogenetic divergence rates were calculated using different fossil and biogeographic calibrations, which are detailed in Appendix 2. Alternative calibrations for the CDT included an expansion that occurred early in the Holocene (8 ka), as well as another during the previous glacial-interglacial transition (~130 ka). In both scenarios, I simply considered that the median values for the HPD of the TEM transition corresponded to 8 and 130 ka, respectively.

## RESULTS

### *Variation of temperature over the last 25 kyrs*

Variations in temperature over the last 25,000 years show post-glacial warming with a positive rate of change from 19.8 to 10.0 ka (12.1 ka in average; Fig. 2) and a maximum increase at two peaks (15.3 and 11.3 ka) separated by a period of relative stability, which included the Younger Dryas. The rate of temperature change was normalised with two half-

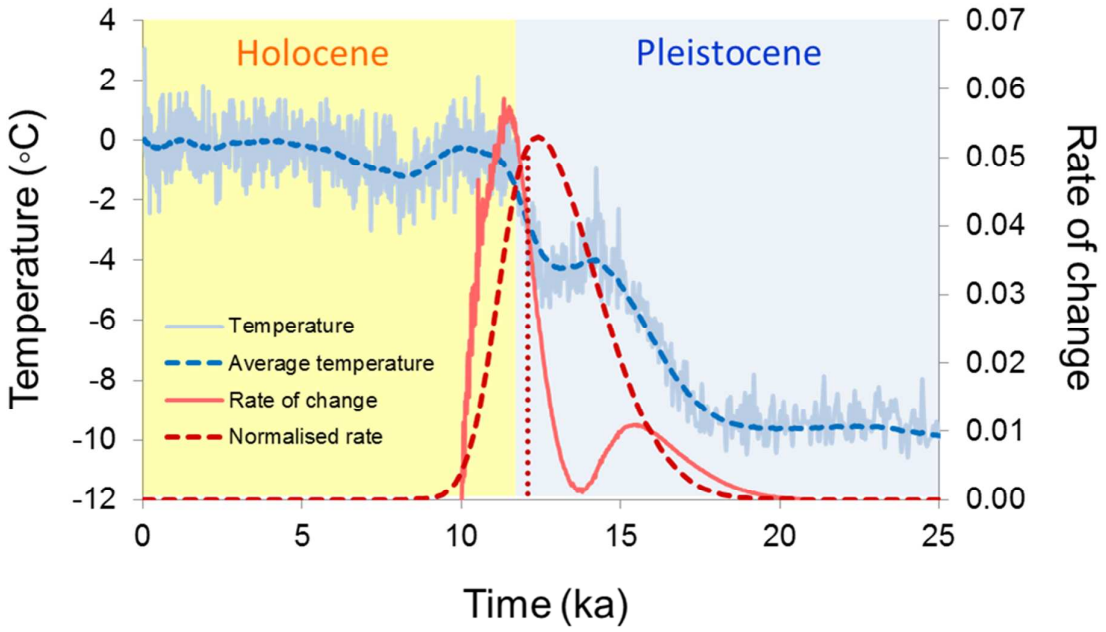


**Figure 2.** Variation of temperature over the last 25 kyrs. Rough temperature data were recovered from deuterium measurement data (Jouzel et al. 2007) (solid light blue line), and the average temperature (dashed blue line) was calculated using a triangular smoothing algorithm over 51 points. The rate of change (solid red line) was calculated from the average temperature curve over time using the equation [($T2$-$T1$)/($t2$-$t1$) with $T$: temperature and t: time]. A normalised curve of the rate of change (dashed red line) was obtained using two half-normal curves using the average time of change (12.1 ka; dashed vertical line), and the 95% confidence interval limits (10.5 and 16.3 ka) of the frequency distribution of the original rate of change occurring between 20 and 10 ka. The Holocene limit (11.7 ka) is illustrated according to Walker et al. (2009). The rate of change of the temperature is bimodal with a first peak at around 15.3 ka before the temperature reaches a plateau and a second higher peak at around 11.3 ka.

normal curves using the average time of change (12.1 ka; dashed vertical line; Fig. 2) and its 95% confidence interval (10.5 to 16.3 ka).

*Validation using simulations*

The uncalibrated TEM applied to the simulated datasets coincides with the change in *Ne* revealed by the BSP (online Appendix 3). The TEM model is therefore adequate to extract the mutations arising since the demographic change. The calculated CDT rates for the simulated data were, on average, larger than the CSE rates, and smaller than the CPC rates (online Appendix 4). Linear correlations were observed between the CDT and the CSE rates, as expected ($R^2 = 1$), but not with the CPC rates ($R^2 = 0.0492$ for 2500 bp; $R^2 = 4.0E\text{-}6$ for 500 bp) (Fig. 3). For the same calibration method and the same genetic content, the rate estimates show large variability between different simulated datasets (online Appendix 4). These results also show that rates obtained using 500 nucleotides have larger confidence intervals than those from 2500 nucleotides. Additional simulations with varying genetic resolution confirmed that the confidence intervals are broader with lower information content (online Appendix 5).

Using the CDT rates, the time-calibrated expansions obtained using BSPs coincide with the dates of the demographic proxy (Fig. 4a-b): *Ne* increases with the increase in temperature between 20 ka and 10 ka. This association is particularly pronounced for the complete dataset (2500 bp), where it is possible to detect the hiatus in the population growth associated with the Younger Dryas. Applying CSE rates, all demographic expansions preceded the increase in temperature (Fig. 4c-d), while, when using the CPC rates, the onsets of the expansions were scattered, but mostly occurred several thousand years after the transition in temperature (Fig. 4e-f).

*Empirical datasets*

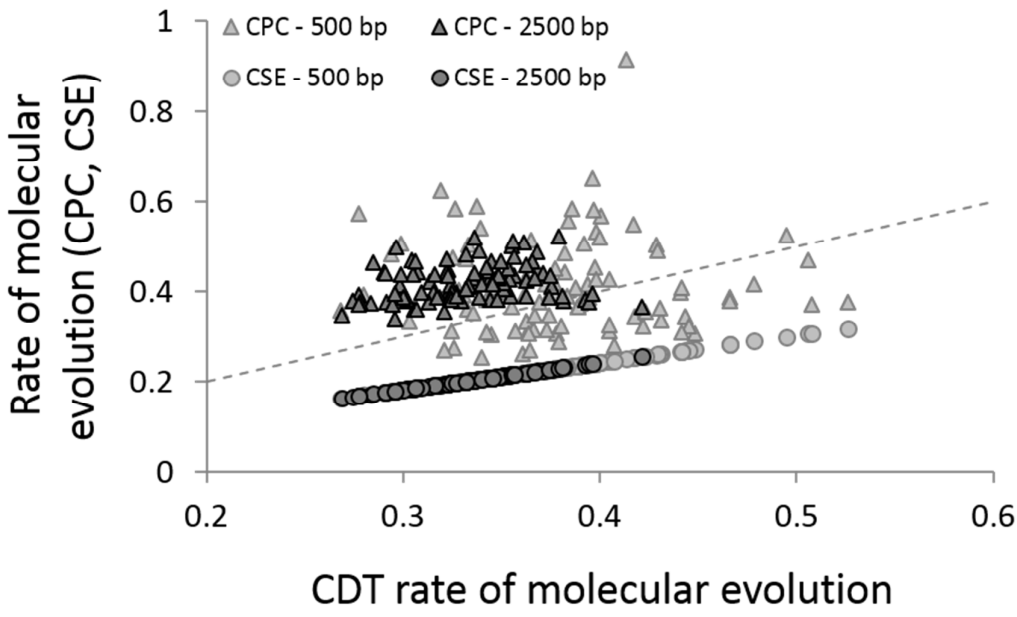


**Figure 3.** Rates obtained from the CDT method relative to alternative calibration methods,based on the start of the expansion (CSE) or on the population coalescent time (CPC). There is a linear relationship between CDT and CSE ($R^2$ = 1), but not between CDT and CPC ($R^2$ =0.0492 for 2500 bp; $R^2$ = 4.0E-6 for 500 bp).

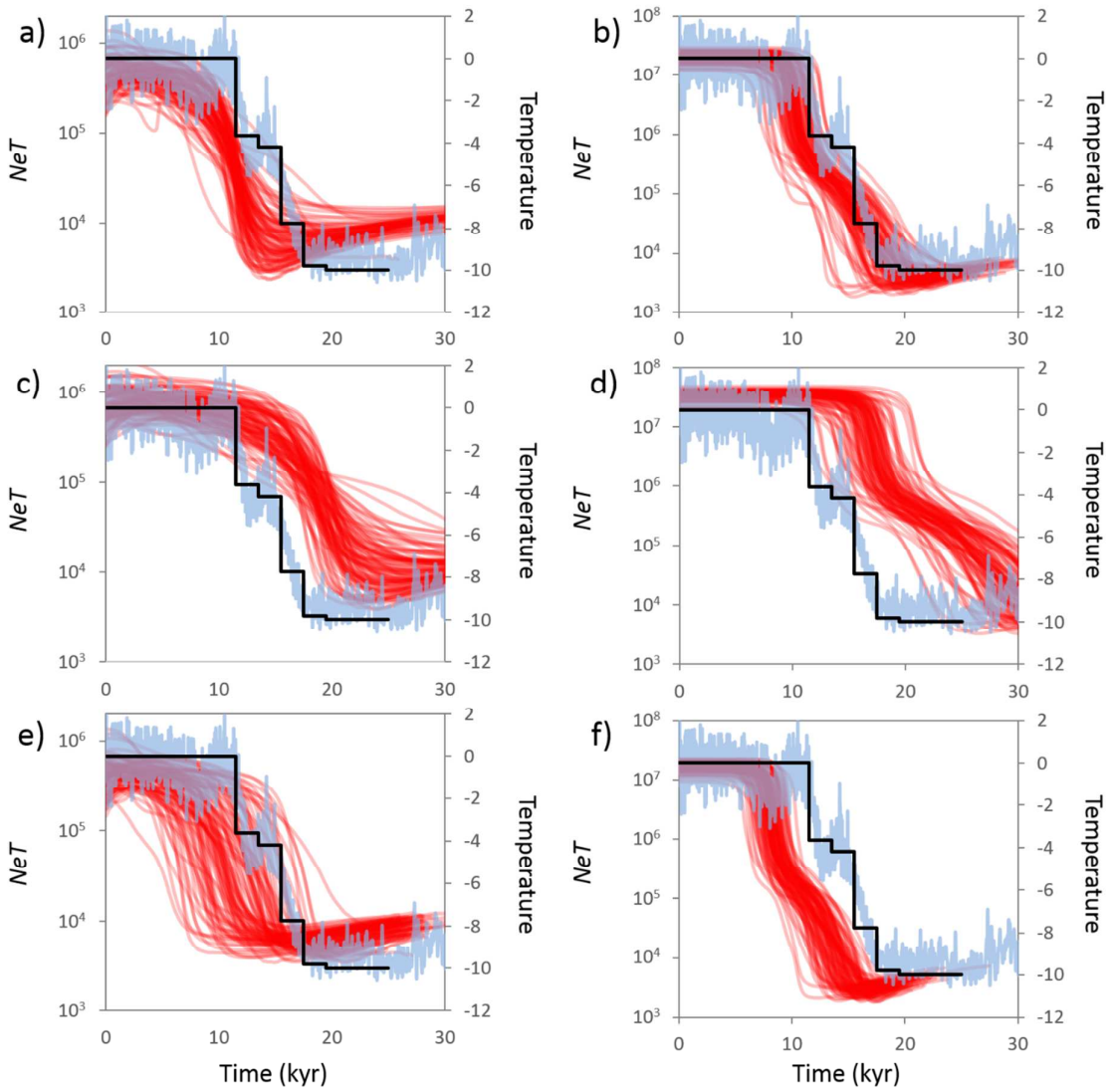


**Figure 4.** Evolution of effective population size (*Ne*T; red curves) and variation of temperature (demographic proxy; blue curves) over the last 30,000 years for different calibration methods, including the CDT method (**a-b**), the CSE method based on the start of the expansion (**c-d;** Crandall et al. 2012), and the CPC method based on the calibration of the *TMRCA* at 20 ka (**e-f**). The black curve in each graph represents the demographic scenario used for the simulations. The graphs on the left hand side (**a, c** and **e**) represent 100 sequences of 500 bp, and the graphs on the right hand side (**b, d** and **f**) represent 100 sequences of 2500bp. The CSE rate overestimates both the time parameters and Ne, while the CPC rate underestimates them. Using higher genetic resolution, the BSP can recover the hiatus in population growth that interrupted the expansion during the Younger Dryas.

Convergence was achieved for each dataset, with all ESS values larger than 200. The strict clock and the TEM had the strongest support from the Bayes factor analyses (online Appendix 6), with the exception of the stickleback, for which it was not possible to reject a model of constant population size and uncorrelated relaxed clock with a lognormal distribution. This dataset also presented the least genetic information content.

The CDT rates ranged from 0.036 for the mtDNA COI gene in the bark beetle to 0.139 for COI in the chocolate chip starfish (Table 1 and Fig. 5). The phylogenetically estimated divergence rates were lower and ranged from 0.009 for COI in the bark beetle to 0.028 for mtDNA control region in humans. The alternative calibration, assuming Holocene expansion, provided higher rates ranging from 0.056 (for the bark beetle) to 0.189 (chocolate chip starfish). The calibration based on the previous glacial-interglacial transition period (130 ka) gave low rates ranging from 0.003 to 0.012 (Table 1; Fig. 5). Calibration of the BSPs using CDT rates gave the expected increase in population between 20 ka and 10 ka. In comparison, phylogenetically calibrated divergence rates suggested earlier increases in *Ne*, mostly coinciding with the glacial period (Fig. 6).

## DISCUSSION

### *Validation of the CDT method*

Simulation studies have proven essential to evaluate performance and properties of newly developed genetic approaches (Hoban et al. 2012). They are used here to validate calibration of the molecular clock using the rate of postglacial temperature transition as an estimate of change in population size (CDT method). The close match of coalescent genealogies with this environmental proxy corroborates the utility of the two-epoch model

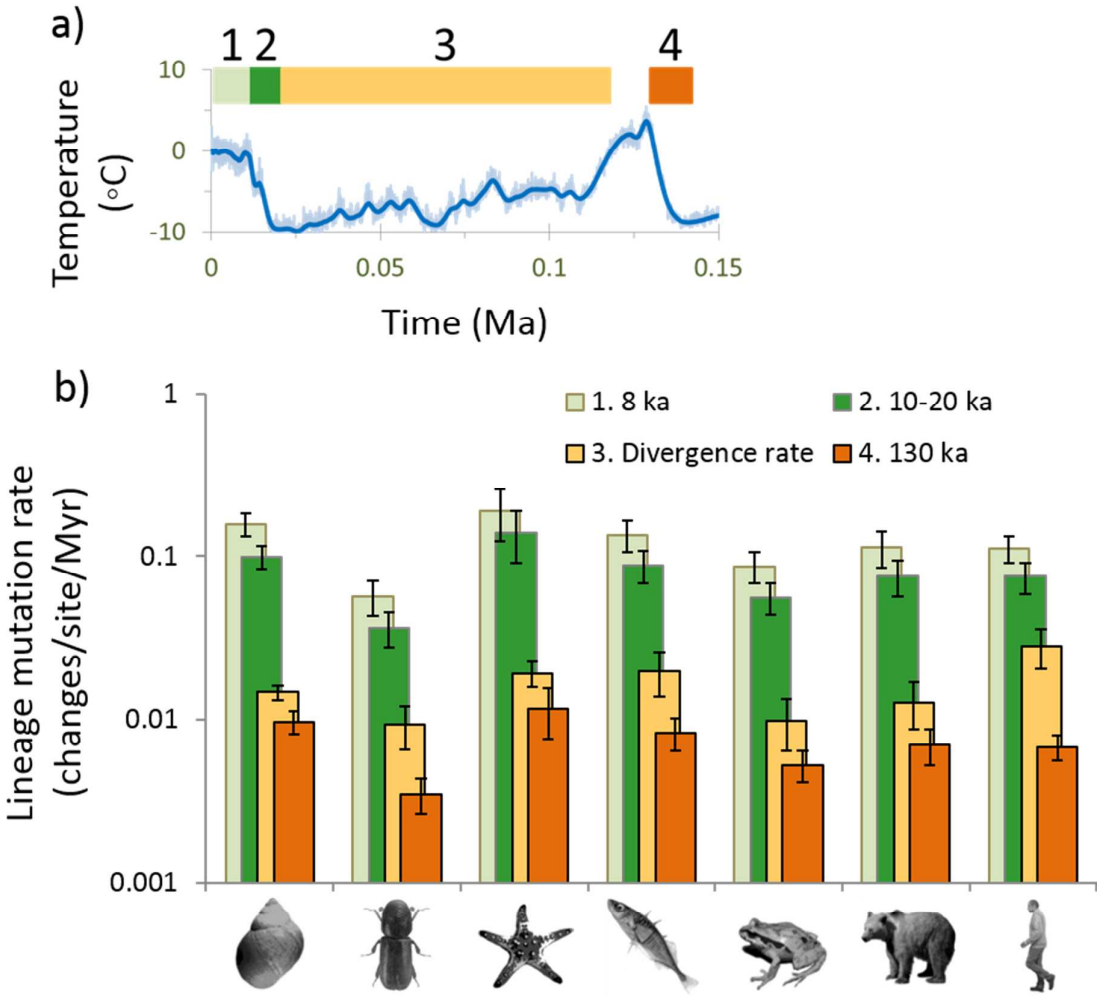


**Figure 5**. Variation of temperature over the last 150 ka with indication of the alternative periods of demographic expansions **(a),** and associated molecular rate estimates obtained for the empirical data, using various calibration dates **(b).** 8 ka: expansion assumed to occur during the Holocene; 10–20 ka: expansion assumed to occur during the post–LGM warming event (CDT rate); >1 myr: older calibration points ranging from 1.5 to 90.0 myrs (divergence rates); 130 ka: expansion assumed to occur during the previous glacial-interglacial transition; From left to right: 1. L*ittorina saxatilis* (Gastropoda: Littorinidae), 2. *Pityogenes chalcographus* (Coleoptera: Curculionidae), 3. *Protoreaster nodosus* (Valvatida: Oreasteridae), 4. *Gasterosteus aculeatus* (Gasterosteiformes: Gasterosteidae), 5. *Eupsophus calcaratus* (Anura: Alsodidae), 6. *Ursus arctos* (Carnivora: Ursidae), 7. *Homo sapiens (*Primates: Hominidae)

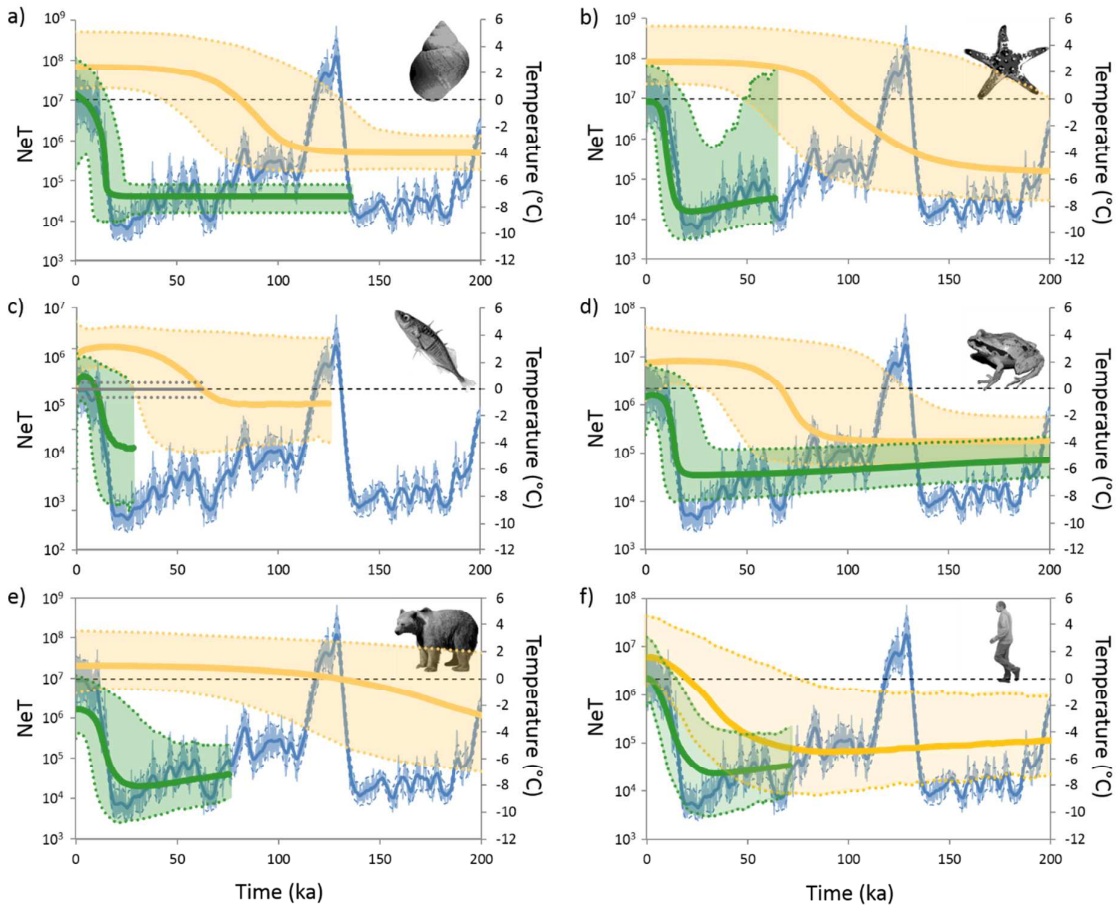


**Figure 6.** Bayesian Skyline plots (BSP) for different species calibrated using the CDT (green) and phylogenetic divergence rates (orange) and change in temperature (blue) over the last 200 Kyrs (from Jouzel et al. 2007). The thick and dashed lines on the BSP represent the median values and 95% confidence intervals of the product of the generation time (*T*) and the effective population size (*Ne*). All the BSPs calibrated using the CDT rate show a demographic expansion that matches the post–LGM increase in temperature between 10–20 ka. a. *Littorina saxatilis* (Gastropoda:Littorinidae), b. *Protoreaster nodosus* (Valvatida:Oreasteridae), c. *Gasterosteus aculeatus* (Gasterosteiformes:Gasterosteidae), d. *Eupsophus calcaratus* (Anura:Alsodidae), e. *Ursus arctos* (Carnivora:Ursidae), f. *Homo sapiens* (Primates:Hominidae).

**Table 1.** Characteristics of the empirical datasets used in the study, estimated demographic transition time and associated rates of molecular evolution calculated for different calibration methods.

| Dataset | Locus / Sequence length (bp) / Sample size | Molecular evolution model | Origin of dataset | Estimated transition time (95% Highest Posterior Density) | CDT rate (95% confidence interval) | Divergence rate ± standard deviation | CSE rate (95% confidence interval) | CPC rate (95% confidence interval) |
|---|---|---|---|---|---|---|---|---|
| Rough periwinkle *Littorina saxatilis* | cyt b / 502-671 / 99 | HKY | Doellman et al. 2011; Panova et al. 2011 | 0.00134 (0.00095–0.00162) | 0.1127 (0.0679 – 0.1448) | 0.0146 ± 0.0015 | 0.1671 (0.1182 – 0.2024) | 0.4093 (0.2702 – 0.5963) |
| Bark beetle *Pityogenes chalcographus* | COI / 564 / 475 | HKY+G | Bertheau et al. 2013 | 0.00046 0.00028–0.00070) | 0.0390 (0.0214–0.0616) | 0.0093 ± 0.0028 | 0.0578 (0.0351 – 0.0876) | 0.5302 (0.3232 – 0.8393) |
| Chocolate chip starfish *Protoreaster nodosus* | COI, tRNAs / 690-866 / 87 | HKY+G | Crandall et al. 2012 | 0.00160 (0.00104–0.00343) | 0.1352 (0.0731–0.2982) | 0.0191 ± 0.0033 | 0.2004 (0.1303 – 0.4288) | 0.2247 (0.1347 – 0.3669) |
| Three-spined stickleback *Gasterosteus aculeatus* | cyt b / 964 / 86 | HKY+G | Mäkinen and Merilä 2008 | 0.00112 (0.00068–0.00174) | 0.0942 (0.0527-0.1508) | 0.0198 ± 0.0060 | 0.1396 (0.0856 – 0.2174) | 0.0789 (0.0484 – 0.1338) |
| Patagonian frog *Eupsophus calcaratus* | cyt b / 698 / 87 | HKY | Nuñez et al. 2011 | 0.00063 (0.00046–0.00098) | 0.0532 (0.0327-0.0854) | 0.0098 ± 0.0034 | 0.0788 (0.0578 – 0.1225) | 0.1974 (0.1155 – 0.3118) |

| | | | | | | | | |
|---|---|---|---|---|---|---|---|---|
| European brown bear *Ursus arctos* | CR, tRNA / 662-667 / 50 | HKY+G | Korsten et al. 2009 | 0.00094 (0.00058–0.00148) | 0.0796 (0.0438-0.1282) | 0.0128 ± 0.0041 | 0.1180 (0.0722 – 0.1847) | 0.1379 (0.0691 – 0.2511) |
| Danish human *Homo sapiens sapiens* | CR / 1121-1129 / 100 | HKY+G | Li et al. 2014 | 0.00089 (0.00056–0.00121) | 0.0747 (0.0426-0.1073) | 0.0280 ± 0.0077 | 0.1107 (0.0702 – 0.1507) | 0.1543 (0.0971 – 0.2381) |

Notes: The estimated transition time between ancestral and modern *Ne* (two-epoch coalescent model) is expressed as a percentage of changes/site. The molecular rate estimates are expressed as a percentage of changes/site/myr. The CDT and CSE rates are calibrated assuming an expansion around 10–20 ka and 19.6 ka, respectively. The CPC rates are calibrated assuming a *TMRCA* at 20 ka. The Appendix 2 details the calculation for the divergence rates.

(TEM) for recovering the number of mutations since this demographic transition (Fig. 1c; online Appendix 3). Consequently, this demonstrates the value of this approach for time calibration within species, as already suggested by Crandall et al. (2012).

The correct association between the genetically inferred demographic transition and temperature variation illustrates that the CDT method provides an accurate calibration, given the assumptions of a post-LGM expansion (20–10 ka), in synchrony with increase in temperature (Fig. 4a-b). According to population genetics theory, rates of molecular evolution, calculated over shorter time scales, are expected to be inflated due to the incorporation of segregating polymorphism (Peterson and Masel 2009; Charlesworth 2010; Mugal et al. 2014). The CDT-derived rate of molecular evolution incorporates segregating polymorphism (neutral and slightly deleterious) in its calculation and thereby reduces calibration biases inherent when using phylogenetic calibrations to date population history. As such, it can be defined as the rate calculated using all new mutations arising in the genealogy of the population sample (all sampled branches) since the time of the demographic transition (in this case, the expansion).

Considering the specific timeline of the CDT calibration (10–20 ka), the new rates are likely different from others based on alternative calibration dates. For instance, the CDT method contrasts with calibration using CSE rates (e.g. Crandall et al. 2012), which is based on the start of the expansion and results in a dissociation between demographic and temperature changes (Fig. 4c-d). These results illustrate the necessity of incorporating the full variability of change in an environmental proxy to correctly calibrate demographic expansions. However, the level of inaccuracy for the CSE rates appears moderate when compared to phylogenetically derived divergence rates, which are calculated between species that have accumulated fixed differences (substitutions). As substitutions accumulate at a slower pace than implied by polymorphism within a population, divergence rates are found to

be lower than genealogy-based rates, and their use causes a large overestimation of population parameters (e.g. Ho et al. 2008). Yet, they are still extensively used to calibrate demographic events (Ho et al. 2005; Ho et al. 2007; Ho et al. 2008).

The calibration of population coalescent time (CPC) is often used to obtain intraspecific mutation rates in humans by calibrating the *TMRCA* of specific haplogroups with archaeologically-based estimates of time of first settlement in different regions of the world (Endicott and Ho 2008; Henn et al. 2009; Subramanian 2009). The application of this method to the simulated datasets showed rates that were most often higher than the CDT rates (Fig. 3; online Appendix 4), causing substantial underestimation of time and population parameters (Fig. 4e-f). Considering that the CPC method uses older calibration dates than the CDT method, lower rates could be expected. Here, the inflated CPC rates are more likely explained by the consistent discordance between deep coalescence (*TMRCA*) and more recent age of populations (Rannala, 1997). Theoretically, accuracy of the CPC method depends on the synchrony between the deepest coalescence in the genealogy and the population age, which happens only under drastic bottlenecks and founding effects (Rannala, 1997). Even though more appropriate than divergence rates, CPC rates cannot be confidently applied to calibrate demographic events.

Calibration methods based on pedigree and heterochronous sampling are similar to CDT rates as they are also calculated using segregating polymorphism within a genealogy. However, as these alternative methods are based on more recent timeframes, with higher stochastic variance and a higher load of deleterious alleles contributing to standing polymorphism, they result in inferred rates that are substantially higher (Charlesworth 2010; Mugal et al. 2014). Derived over only a few generations, pedigree rate is less affected by allele fixation (i.e. less genetic drift and selection), which results in estimates that are close to the instantaneous rate (Ho et al. 2011a). For heterochronous sampling, providing that serially

sampled viruses or aDNA of good quality are available (i.e. distinct ages and spread over an adequate temporal range), it is possible to use the accumulation of genetic variation over time to estimate a molecular rate (Rambaut 2000; Drummond et al. 2003). This method gives access to variants that are either extinct, or fixed in the current population, which results in very high estimates of mutation rate. These rate estimates are most often specific to a given dataset, which limits rate transferability for these alternative genealogy-based calibration methods.

The results show that genetic information content can have a substantial effect on the rate estimates and the resolution of time and population parameters. Rates are overestimated for shorter sequences (online Appendix 4), which leads to underestimation of expansion timing and smaller *Ne* estimates (Fig. 4a-b). Studies based on aDNA found similar results, with low genetic content associated with wider rate uncertainty, causing an upward bias in the rate estimates (Howell et al. 2007; Debruyne and Poinar 2009; Firth et al. 2010; Ho et al. 2011b). Additional simulations showed that despite low precision in rate estimates with less genetic data, the true value is still included (online Appendix 5), which suggests limited errors. This is confirmed by simulation results as the calibration still provides fairly good approximations of the parameter estimates (Fig. 4a). Both randomness of mutations and evolutionary stochasticity of the coalescent process create a large variance in rate estimates, exacerbated by low genetic information content. This warrants caution on the transferability of molecular rates when derived from and applied to datasets with significantly different genetic content. The Younger Dryas event was detected only using the complete simulated dataset (Fig. 4a-b), which also suggests that the information content influences the resolution of demographic signal.

*Empirical Data and Rate Heterogeneity Over Time*

Molecular rates estimated for the different species were three to seven times higher for the CDT rates than for the divergence rates previously applied to each taxon (Table 1; Fig. 5). Most of these rates were lower than those obtained using control region sequences based on aDNA in brown bear (0.30 changes/site/myr; Korsten et al. 2009), internal calibration of human (about 0.30 changes/site/myr; Endicott and Ho 2008) or corrected for time dependency for modern humans (0.0988 changes/site/myr; Soares et al. 2009). This pattern of rate differences supports the hypothesis of time dependency of inferred molecular rates predicting increased values converging towards instantaneous rates when using recent calibration dates (Ho et al. 2005).

Despite theoretical and empirical corroboration, the hypothesis of time dependency of evolutionary rates suffers from considerable controversy due to multiple confounding factors that may inflate estimates for recent rates (review in Ho et al. 2011a). Some of these factors are linked to calibration methods including uncertainties due to ancestral polymorphism (Peterson and Masel 2009), as well as uncertainties of both dates of biogeographic events (Emerson 2007; Lessios 2008; Henn et al. 2009) and phylogenetic positions of fossils (Ho et al. 2011a). Others are linked to misspecifications of the substitution model (Sullivan and Joyce 2005; Emerson 2007; Howell et al. 2007; Raquin et al. 2008), inadequacy of demographic models (Navascues and Emerson 2009; Balloux and Lehmann 2012) and selective constraints on the studied genes (Subramanian and Lambert 2011; Duchene et al. 2014). Genetic information content also causes inflated rates depending on patterns of inheritance (Ho et al. 2011a), saturation of markers (Raquin et al. 2008; Duchene et al. 2014), ascertainment bias (Zhivotovsky et al. 2004; Bandelt 2008; Ballantyne et al. 2010), sampling design (Emerson 2007; Bandelt 2008), sequence errors (Clark and Whittam 1992; Ho et al. 2005; Johnson and Slatkin 2008), skewed rate distribution (Heled and Drummond 2008;

Debruyne and Poinar 2009; Ho et al. 2011b), small sequence sizes (Debruyne and Poinar 2009; present study), and limited number of sequences (present study).

The CDT method circumvents and addresses some of these drawbacks: 1) the phylogeographic expectations of the contraction-expansion model can provide an accurate demographic calibration (see discussion on Phylogeographic Cross-Checking); 2) the issue of a simplistic model is reduced as BSP analysis is an extremely flexible coalescent model, able to reconstruct changes in *Ne* through time (Pybus et al. 2000; Ho and Shapiro 2011 for a review); 3) by enabling the estimation of a molecular rate for each taxon, the CDT method allows an independent estimate of the rates, which greatly reduces problems related to genetic information content.

*Rate comparison between species*

As the calibration is based on the same climatic events for all species, it provides a unique opportunity to compare molecular rates between taxa. Substantial differences in molecular evolution are revealed between species at the cytochrome *b* gene and the mitochondrial control region (Table 1). Remarkably, even though the molecular rate of the control region is commonly known to be faster than the rest of the mitochondrial genome (e.g. Endicott and Ho 2008), the inferred rate for humans and brown bears were lower than most rates obtained for protein-coding genes in other species (Table 1). Multiple covarying biological factors may explain this reduced molecular rate in large mammals, including large body size, long generation time, and relatively slow metabolism (Baer et al. 2007; Bromham 2011).

In the light of the generation–time (Wu and Li 1985) and metabolic–rate hypotheses (Martin and Palumbi 1993), the molecular rate of the bark beetle is low (0.0362 changes/site/myr) compared to other taxa. According to these hypotheses, organisms with

small body size, short generation time and high fecundity should be characterized by higher mutation rates. The low rate likely indicates an inappropriate CDT calibration, due to failure of the proxy assumptions, and suggests an expansion occurring later during the Holocene. This dataset was excluded in further analyses. Therefore, not all expansions correspond to the late glacial period and this warrants caution in the application of the CDT method. Considering the sensitivity of the demographic rate estimates to genetic information content, errors should be estimated by simulation for varying datasets (*e.g.* number and length of sequences) for reliable rate comparisons.

The comparative study of molecular rates among taxa faces several important challenges (Lanfear et al. 2010), some of which can be addressed by the CDT method. Substitution rates estimated from branch length methods and traditionally used to compare rates between species, are associated with large uncertainties (Lanfear et al. 2010). The assumptions upon which the CDT method is based provide a robust calibration that should improve rate comparison. A related issue is the non-independence of the statistical methods used to estimate substitution rates (Lanfear et al. 2010), which is addressed in the CDT method by providing a distinct calibration for each taxon. Finally, due to the broad applicability of the method, rate comparison, largely limited to mammals, can now be applied to a much larger number of taxa (Bromham 2011).

### *Phylogeographic Cross-Checking*

Despite the overwhelming consensus in the literature (see Hewitt 2000 and Provan and Bennett 2008 for reviews), it is challenging to demonstrate that the environmental conditions of the late glacial period were the triggers of demographic expansions. First of all, it is not possible to know the true demographic history. Other confounding factors could also

be involved (e.g. competition or disease). Therefore, making the false assumption of an expansion during the post-glacial period is a potential limitation of the CDT method. To evaluate the hypothesis, I compared it to alternative timings of expansion, by exploring for each period the ecological requirements and demographic assumptions associated with the environmental factors at play, and the reliability of the resulting rates.

Several lines of supporting evidence suggest that the greatest demographic expansions occurred during the postglacial warming period, while others reveal incongruences when considering alternative calibration dates. Demographic expansions occurring simultaneously in a large number of species are best explained by major ecological changes in the whole ecosystem, resulting in the expansion of refugia and the creation of new habitats. In recent evolutionary history, these ecological conditions are found during climate warming that occurred between 20–10 ka (Fig. 2), which led to an expansion in most temperate species, including those in the present study. In humans for instance, both archaeological remains (Gamble et al. 2005) and aDNA-based surveys (e.g. Olivieri et al. 2013), have identified the same timeline for the expansion, resulting in the colonization of Europe from southern refugia.

When calibrated using divergence rates, all the expansions obtained for the empirical datasets appear to be scattered across the glacial period (110–20 ka). During glacial periods, terrestrial and marine habitats of the species considered were probably restricted. These habitats were unlikely to have experienced the extensive increase causing demographic expansions, inferred in the present study, given the marine regression and the presence of ice sheets covering much of Northern Europe, Northern North America and Southern South America (Denton et al. 2010). Moreover, evidence based on both theoretical population genetics (Peterson and Masel 2009) and empirical results (Ho et al. 2008; Ho et al. 2011a), suggests that divergence rates overestimate time and demographic parameters estimated using

genetic variation within population samples. Therefore, molecular rates that date expansions during glacial periods are probably inappropriate for these species.

If expansions occurred at the beginning of the Holocene (8 ka), the estimated molecular rates are moderately larger (~50%) than the CDT rates (Table 1; Fig. 5). However, when considering the glacial period, the relative ecological stability observed during the Holocene challenges the idea of simultaneous expansion of numerous species. These rates are therefore, probably also inexact.

The previous glacial–interglacial period (~130 ka) is the only alternative calibration date that meets the ecological requirements for multiple simultaneous expansions. If this is considered, two distinct expansions associated with the two glacial-interglacial transitions should be recovered from the demographic reconstructions. Alternatively, if a strong bottleneck occurs during the glacial period, the older demographic signature disappears and only the more recent expansion can be detected (online Appendix 6; Grant and Cheng 2012; Grant et al. 2012). The latter fits better with the demographic patterns observed in the empirical datasets (Fig. 6). Finally, this calibration provides rates that are one order of magnitude smaller than CDT rates and consistently smaller than divergence rates (Table 1; Fig. 5). Such strong inconsistencies suggest that the post-LGM warming period is the best time line for calibration of these demographic expansions.

Since BSP analyses are based on coalescent theory, violation of the assumption of panmixia may lead to distortion in various population parameter estimates (Ho and Shapiro 2011). Several theoretical studies have recently shown that the inference of past demography using subdivided populations, can result in the detection of false positive population declines (Nielsen and Beaumont 2009; Städler et al. 2009; Chikhi et al. 2010; Peter et al. 2010; Heller et al. 2013). As in a population bottleneck, the increase in migration within a population also

creates a higher rate of coalescent events in the recent part of the genealogy (i.e. scattering phase; Wakeley 1999), which results in a structure effect (Heller et al. 2013). It is important to sample multiple populations evenly to minimize the structure effect, because larger genetic declines are inferred when focussing on local sampling (Heller et al. 2013). Incorporating populations with asynchronous expansions may represent another source of bias in demographic reconstruction. This could affect the precision of time and population parameters, by broadening the confidence intervals of the rate estimates. In the present study, the empirical datasets were chosen from specific populations or haplogroups, and none of them showed signs of genetic decline or specifically low precision of the parameters (Fig. 6). Therefore, even though it is impossible to rule out admixture within the empirical datasets, it is reasonable to assume that the absence of bottleneck signals is a robust argument against substantial consequences of genetic structure.

## CONCLUSIONS

The genomic era offers access to large amounts of genetic data which has the potential to greatly improve the precision of time and population estimates, but this development is associated with several important challenges. Statistical and computational challenges will mainly be addressed by the improvement of phylogenetic methods and the development of computer resources (Ho 2014). On the other hand, the estimation of an accurate molecular clock is an important issue that needs to be addressed as it determines the accuracy of time and population estimates. By matching demographic history and ecological changes, the CDT method deals with the rate discrepancy between species divergence and population events. It does so by providing a molecular clock that incorporates segregating polymorphisms, which partly explain the apparent acceleration of the rate on short timescales (Petersen and Masel 2009). The new method represents a framework to study heterogeneity

of rates of molecular evolution and further evaluate their variation according to either genetic content, taxon or calibration time.

These results also reinforce the importance of the Pleistocene contraction-expansion model, which provides a framework to better understand the role of environmental factors on the demography of temperate species. New questions arise related to organisms that show more subtle association with climatic changes, but reconstruction of historical species distribution offers some perspectives on this. For instance, a recent study showed a large increase in tropical shallow water habitats (<60 m) associated with the rise in sea level since the LGM (Ludt and Rocha 2015). This suggests that a large fraction of tropical marine species may have also experienced substantial expansions over this period. Moreover, providing that high-resolution genetic markers are used, more subtle demographic signatures will be identified (e.g. reduced expansion during the Younger Dryas), which will help in validating the method using empirical data. Before these are investigated in depth, the application of the CDT method to other organisms should still provide a better calibration than the divergence rates.

The potentially incorrect assumption of an expansion during the postglacial warming period is probably the main limitation of the method, which could result in inaccurate time and population estimates. As illustrated in the bark beetle example, it is recommended that a combination of multiple independent lines of evidence (ecology, environmental proxies and rate comparisons) is used to confirm whether or not the calibration is appropriate for a new taxon. Alternative events could be considered, such as those that led to recent extinctions or bottleneck in numerous species (e.g. explosion of Mount Toba; Williams et al. 2009). Low genetic information content is another limit of the method since it inflates estimates of molecular rates and broadens their confidence intervals. Providing that robust demographic assumptions and high–resolution genetic data are used, the method provides accurate

demographic reconstruction over recent time frames, especially for species of conservation concern.

## SUPPLEMENTARY MATERIAL

Data available from the Dryad Digital Repository (doi:10.5061/dryad.7c65g).

## ACKNOWLEDGMENTS

The author thanks P. Bloomer, and E. Boissin for useful discussions, E. Crandall for helping with the two-epoch model in an early stage of the work, and the Research and Innovation Support of University of Pretoria. The author is grateful to M. Cunningham, S.Y.W. Ho and K. Reid for providing constructive comments on earlier drafts of the manuscript. TBH was supported by the Department of Science and Technology African Coelacanth Ecosystem Programme (ACEP) II and the Research Development Programme of the University of Pretoria.

## REFERENCES


Baele G, P. Lemey, T. Bedford, A. Rambaut, M.A. Suchard, and A.V. Alekseyenko. 2012. Improving the Accuracy of Demographic and Molecular Clock Model Comparison While Accommodating Phylogenetic Uncertainty. Mol. Biol. Evol. 29:2157–2167.

Baer, C.F., M.M. Miyamoto, and D.R. Denver. 2007. Mutation rate variation in multicellular eukaryotes: causes and consequences. Nat. Rev. Genet. 8:619–631.

Bagley, J.C., M. Sandel, J. Travis, M. de Lourdes Lozano–Vilano, and J.B. Johnson. 2013. Paleoclimatic modeling and phylogeography of least killifish, *Heterandria formosa*: insights into Pleistocene expansion–contraction dynamics and evolutionary history of North American Coastal Plain freshwater biota. BMC Evol. Biol. 13:223.

Bakke, J., O. Lie, E. Heegaard, T. Dokken, G.H. Haug, H.H. Birks, P. Dulski, and T. Nilsen. 2009. Rapid oceanic and atmospheric changes during the Younger Dryas cold period. Nature Geosci. 2:202–205.

Ballantyne, K.N., M. Goedbloed, R. Fang, O. Schaap, O. Lao, A. Wollstein, Y. Choi, K. van Duijn, M. Vermeulen, S. Brauer, R. Decorte, M. Poetsch, N. von Wurmb-Schwark, P. de Knijff, D. Labuda, H. Vézina, H. Knoblauch, R. Lessig, L. Roewer, R. Ploski, T. Dobosz, L. Henke, J. Henke, M.R. Furtado, and M. Kayser. 2010. Mutability of Y–Chromosomal Microsatellites: Rates, Characteristics, Molecular Bases, and Forensic Implications. Am. J. Hum. Genet. 87:341–353.

Balloux, F., and L. Lehmann. 2012. Substitution rates at neutral genes depend on population size under fluctuating demography and overlapping generation. Evolution 66:605–611.

Bandelt, H.J. 2008. Time dependency of molecular rate estimates: tempest in a teacup. Heredity 100:1–2.

Bertheau, C., H. Schuler, W. Arthofer, D.N. Avtzis, F. Mayer, S. Krumboeck, Y. Moodley, and C. Stauffer. 2013. Divergent evolutionary histories of two sympatric spruce bark beetle species. Mol. Ecol. 22:3318–3332.

Borer M., N. Alvarez, S. Buerki, N. Margraf, M. Rahier, qnd R.E. Naisbit. 2010. The phylogeography of an alpine leaf beetle: Divergence within Oreina elongata spans several ice ages. Mol. Phyl. Evol. 57:703–709.

Bromham, L. 2011. The genome as a life–history character: why rate of molecular evolution varies between mammal species. Philos. Trans. R. Soc. Lond. B Biol. Sci. 366:2503–2513.

Brotherton P, W. Haak, J. Templeton, G. Brandt, J. Soubrier, C.J. Adler, S.M. Richards, C.D. Sarkissian, R. Ganslmeier, S. Friederich, V. Dresely, M. van Oven, R. Kenyon, M.B. Van der Hoek, J. Korlach, K. Luong, S.Y.W. Ho, L. Quintana–Murci, D.M. Behar, H. Meller, K.W. Alt, A. Cooper, and The Genographic Consortium. 2013. Neolithic mitochondrial haplogroup H genomes and the genetic origins of Europeans. Nat. Commun. 4:2656.

Brown, W.M., M. George, and A.C. Wilson. 1979. Rapid evolution of animal mitochondrial–DNA. Proc. Natl. Acad. Sci. U.S.A. 76:1967–1971.

Burridge, C.P., D. Craw, D. Fletcher, and J.M. Waters. 2008. Geological dates and molecular rates: Fish DNA sheds light on time dependency. Mol. Biol. Evol. 25:624–633.

Charlesworth, D. 2010. Don't forget the ancestral polymorphism. Heredity 105:509–510

Chikhi, L., V.C., Sousa, P. Luisi, B. Goossens, and M.A. Beaumont. 2010. The Confounding Effects of Population Structure, Genetic Diversity and the Sampling Scheme on the Detection and Quantification of Population Size Changes. Genetics 186:983–U347.

Clark, A.G., and T.S. Whittam. 1992. Sequencing errors and molecular evolutionary analysis. Mol. Biol. Evol. 9:744–752.

Cornuet, J.–M., V. Ravigne, and A. Estoup. 2010. Inference on population history and model checking using DNA sequence and microsatellite data with the software DIYABC (v1.0). BMC Bioinformatics 11:401.

Crandall, E.D., E.J. Sbrocco, T.S. DeBoer, P.H. Barber, and K.E. Carpenter. 2012. Expansion Dating: Calibrating Molecular Clocks in Marine Species from Expansions onto the Sunda Shelf Following the Last Glacial Maximum. Mol. Biol. Evol. 29:707–719.

Crawford, A.J. 2003. Relative rates of nucleotide substitution in frogs. J. Mol. Evol. 57:636–641.

Debruyne, R., and H.N. Poinar. 2009. Time Dependency of Molecular Rates in Ancient DNA Data Sets, A Sampling Artifact? Syst. Biol. 58:348–359.

Denton, G.H., Anderson R.F., Toggweiler J.R., Edwards R.L., Schaefer J.M., and A.E. Putnam. 2010. The Last Glacial Termination. Science 328:1652–1656.

Doellman, M.M., G.C. Trussell, J.W. Grahame, and V.S. Vollmer. 2011. Phylogeographic analysis reveals a deep lineage split within North Atlantic *Littorina saxatilis*. P. Roy. Soc. B Biol. Sci. 278:3175–3183.

Drummond, A.J., O.G. Pybus, A. Rambaut, R. Forsberg, and A.G. Rodrigo. 2003. Measurably evolving populations. Trends Ecol. Evol. 18:481–488.

Drummond, A.J., and A. Rambaut. 2007. BEAST: Bayesian evolutionary analysis by sampling trees. BMC Evol. Biol. 7:214.

Drummond, A.J., A. Rambaut, B. Shapiro, and O.G. Pybus. 2005. Bayesian coalescent inference of past population dynamics from molecular sequences. Mol. Biol. Evol. 22:1185–1192.

Duchene, S., E.C. Holmes, and S.Y.W. Ho. (2014) Analyses of evolutionary dynamics in viruses are hindered by a time–dependent bias in rate estimates. P. Roy. Soc. B Biol. Sci. 281:20140732.

Emerson, B.C. 2007. Alarm bells for the molecular clock? No support for Ho et al.'s model of time–dependent molecular rate estimates. Syst. Biol. 56:337–345.

Endicott, P., and S.Y.W. Ho. 2008. A Bayesian evaluation of human mitochondrial substitution rates. Am. J. Hum. Genet. 82:895–902.

Firth, C., A. Kitchen, B. Shapiro, M.A. Suchard, E.C. Holmes, and A. Rambaut. 2010. Using Time–Structured Data to Estimate Evolutionary Rates of Double–Stranded DNA Viruses. Mol. Biol. Evol. 27:2038–2051.

Fleischer, R.C., C.E. McIntosh, and C.L. Tarr. 1998. Evolution on a volcanic conveyor belt: using phylogeographic reconstructions and K–Ar–based ages of the Hawaiian Islands to estimate molecular evolutionary rates. Mol. Ecol. 7:533–545.

Fraser, C.I., R. Nikula, D.E. Ruzzante, and J.M. Waters. 2012. Poleward bound: biological impacts of Southern Hemisphere glaciation. Trends Ecol. Evol. 27:462–471.

Fu Q., A. Mittnik, P.L.F. Johnson, K. Bos, M. Lari, R. Bollongino, C. Sun, L. Giemsch, R. Schmitz, J. Burger, A.M. Ronchitelli, F. Martini, R.G. Cremonesi, J. Svoboda, P. Bauer, D. Caramelli, S. Castellano, D. Reich, S. Paabo, and J. Krause. 2013. A Revised Timescale for Human Evolution Based on Ancient Mitochondrial Genomes. Curr. Biol. 23:553–559.

Gamble, C., W. Davies, P. Pettitt, L. Hazelwood, and M. Richards. 2005. The archaeological and genetic foundations of the European population during the late glacial: Implications for 'agricultural thinking'. Camb. Archaeol. J. 15:193–223.

Grant, W.S., and W. Cheng. 2012. Incorporating deep and shallow components of genetic structure into the management of Alaskan red king crab. Evol. Appl. 5:820–837.

Grant, W.S., M. Liu, T. Gao, and T. Yanagimoto. 2012. Limits of Bayesian skyline plot analysis of mtDNA sequences to infer historical demographies in Pacific herring (and other species). Mol. Phyl. Evol. 65:203–212.

Heled, J., and A.J. Drummond. 2008. Bayesian inference of population size history from multiple loci. BMC Evol. Biol. 8:289.

Heller, R., L. Chikhi, and H.R. Siegismund. 2013. The Confounding Effect of Population Structure on Bayesian Skyline Plot Inferences of Demographic History. Plos One, 8:e62992.

Henn, B.M., C.R. Gignoux, M.W. Feldman, and J.L. Mountain. 2009. Characterizing the Time Dependency of Human Mitochondrial DNA Mutation Rate Estimates. Mol. Biol. Evol. 26:217–230.

Herman, J.S., and J.B. Searle. 2011. Post-glacial partitioning of mitochondrial genetic variation in the field vole. P. Roy. Soc. B Biol. Sci. 278:3601–3607.

Hewitt, G. 2000. The genetic legacy of the Quaternary ice ages. Nature 405:907–913.

Ho, S.Y.W. 2014. The changing face of the molecular evolutionary clock. Trends Ecol. Evol. 29:496-503.

Ho, S.Y.W., and P. Endicott. 2008. The crucial role of calibration in molecular date estimates for the peopling of the Americas. Am. J. Hum. Genet. 83:142-146.

Ho, S.Y.W., R. Lanfear, L. Bromham, M.J. Phillips, J. Soubrier, A.G. Rodrigo, and A. Cooper. 2011a. Time–dependent rates of molecular evolution. Mol. Ecol. 20:3087–3101.

Ho, S.Y.W., R. Lanfear, M.J. Phillips, I. Barnes, J.A. Thomas, S.–O. Kolokotronis, and B. Shapiro. 2011b. Bayesian Estimation of Substitution Rates from Ancient DNA Sequences with Low Information Content. Syst. Biol. 60:366–374.

Ho, S.Y.W., and G. Larson. 2006. Molecular clocks: when times are a–changin'. Trends Genet. 22:79–83.

Ho, S.Y.W., M.J. Phillips, A. Cooper, and A.J. Drummond. 2005. Time dependency of molecular rate estimates and systematic overestimation of recent divergence times. Mol. Biol. Evol. 22:1561–1568.

Ho, S.Y.W., U. Saarma, R. Barnett, J. Haile, and B. Shapiro. 2008. The Effect of Inappropriate Calibration: Three Case Studies in Molecular Ecology. PLoS One 3:e1615.

Ho, S.Y.W., and B Shapiro. 2011. Skyline–plot methods for estimating demographic history from nucleotide sequences. Mol. Ecol. Res. 11:423–434.

Ho, S.Y.W., B. Shapiro, M.J. Phillips, A. Cooper, and A.J. Drummond. 2007. Evidence for time dependency of molecular rate estimates. Syst. Biol. 56:515–522.

Hoareau, T.B., E. Boissin, and P. Berrebi. 2012. Evolutionary history of a widespread Indo–Pacific goby: The role of Pleistocene sea–level changes on demographic contraction/expansion dynamics. Mol. Phyl. Evol. 62:566–572.

Hoban, S., G. Bertorelle, and O.E. Gaggiotti. 2012. Computer simulations: tools for population and evolutionary genetics. Nat. Rev. Genet. 13:110–122.

Howell, N., J.L. Elson, C. Howell, and D.M. Turnbull. 2007. Relative rates of evolution in the coding and control regions of African mtDNAs. Mol. Biol. Evol. 24:2213–2221.

Johnson, P.L.F., and M. Slatkin. 2008. Accounting for bias from sequencing error in population genetic estimates. Mol. Biol. Evol. 25:199–206.

Jouzel, J., V. Masson–Delmotte, O. Cattani, G. Dreyfus, S. Falourd, G. Hoffmann, B. Minster, J. Nouet, J.M. Barnola, J. Chappellaz, H. Fischer, J.C. Gallet, S. Johnsen, M. Leuenberger, L. Loulergue, D. Luethi, H. Oerter, F. Parrenin, G. Raisbeck, D. Raynaud, A. Schilt, J. Schwander, E. Selmo, R. Souchez, R. Spahni, B. Stauffer, J.P. Steffensen, B. Stenni, T.F. Stocker, J.L. Tison, M. Werner, and E.W. Wolff. 2007. Orbital and Millennial Antarctic Climate Variability over the Past 800,000 Years. Science 317:793–796.

Kimura, M. 1968. Evolutionary rate at molecular level. Nature 217:624–626.

Korsten M., S.Y.W. Ho, J. Davison, B. Pahn, E. Vulla, M. Roht, I.L. Tumanov, I. Kojola, Z. Andersone–Lilley, J. Ozolins, M. Pilot, Y. Mertzanis, A. Giannakopoulos, A.A. Vorobiev,

N.I. Markov, A.P. Saveljev, E.A. Lyapunova, A.V. Abramov, P. Mannil, H. Valdmann, S.V. Pazetnov, V.S. Pazetnov, A.M. Rokov, and U. Saarma. 2009. Sudden expansion of a single brown bear maternal lineage across northern continental Eurasia after the last ice age: a general demographic model for mammals? Mol. Ecol. 18:1963–1979.

Krause, J., T. Unger, A. Nocon, A.–S. Malaspinas, S.–O. Kolokotronis, M. Stiller, L. Soibelzon, H. Spriggs, P.H. Dear, A.W. Briggs, C.E.S. Bray, S.J. O'Brien, G. Rabeder, P. Matheus, A. Cooper, M. Slatkin, S. Pääbo, and M. Hofreiter. 2008. Mitochondrial genomes reveal an explosive radiation of extinct and extant bears near the Miocene-Pliocene boundary. BMC Evol. Biol. 8:220.

Kumar, S. 2005. Molecular clocks: four decades of evolution. Nat. Rev. Genet. 6:654–662.

Lanfear, R., J.J. Welch, and L. Bromham. 2010. Watching the clock: Studying variation in rates of molecular evolution between species. Trends Ecol. Evol. 25:495–503.

Laurin, M. 2012. Recent progress in paleontological methods for dating the Tree of Life. Front. Genet. 3:130–130.

Lessios, H.A. 2008. The Great American Schism: Divergence of Marine Organisms After the Rise of the Central American Isthmus. Ann. Rev. Ecol. Syst. 39:63–91.

Li S., S. Besenbacher, Y. Li, K. Kristiansen, N. Grarup, A. Albrechtsen, T. Sparso, T. Korneliussen, T. Hansen, J. Wang, R. Nielsen, O. Pedersen, L. Bolund, and M.H. Schierup. 2014. Variation and association to diabetes in 2000 full mtDNA sequences mined from an exome study in a Danish population. Eur. J. Hum. Genet. 22:1040–1045.

Lorenzen, E.D., D. Nogues–Bravo, L. Orlando, J. Weinstock, J. Binladen, K.A. Marske, A. Ugan, M.K. Borregaard, M.T.P. Gilbert, R. Nielsen, S.Y.W. Ho, T. Goebel, K.E. Graf, D. Byers, J.T. Stenderup, M. Rasmussen, P.F. Campos, J.A. Leonard, K.–P. Koepfli, D. Froese, G. Zazula, T.W. Stafford Jr., K. Aaris–Sørensen, P. Batra, A.M. Haywood, J.S. Singarayer, P.J. Valdes, G. Boeskorov, J.A. Burns, S.P. Davydov, J. Haile, D.L. Jenkins,

P. Kosintsev, T. Kuznetsova, X.. Lai, L.D. Martin, H.G. McDonald, D. Mol, M. Meldgaard, K. Munch, E. Stephan, M. Sablin, R.S. Sommer, T. Sipko, E. Scott, M.A. Suchard, A. Tikhonov, R.Willerslev, R.K.Wayne, A. Cooper, M. Hofreiter, A. Sher, B. Shapiro, C. Rahbek, and E. Willerslev. 2011. Species–specific responses of Late Quaternary megafauna to climate and humans. Nature 479:359–U195.

Ludt, W.B., and L.A. Rocha. 2015. Shifting seas: the impacts of Pleistocene sea-level fluctuations on the evolution of tropical marine taxa. J. Biogeogr. 42:25–38.

Mäkinen, H.S., and J. Merilä. 2008. Mitochondrial DNA phylogeography of the three–spined stickleback (*Gasterosteus aculeatus*) in Europe – Evidence for multiple glacial refugia. Mol. Phyl. Evol. 46:167–182.

Marino, I.A.M., J.M. Pujolar, and L. Zane. 2011. Reconciling Deep Calibration and Demographic History: Bayesian Inference of Post Glacial Colonization Patterns in *Carcinus aestuarii* (Nardo, 1847) and *C. maenas* (Linnaeus, 1758). PLoS One 6:e28567.

Martin, A.P., and S.R. Palumbi. 1993. Body size, metabolic–rate, generation time, and the molecular clock. Proc. Natl. Acad. Sci. U.S.A. 90:4087–4091.

Millar, C.D., A. Dodd, J. Anderson, G.C. Gibb, P.A. Ritchie, C. Baroni, M.D. Woodhams, M.D. Hendy, and D.M. Lambert. 2008. Mutation and Evolutionary Rates in Adelie Penguins from the Antarctic. Plos Genet. 4: e1000209.

Mugal, C.F., J.B.W. Wolf, and I. Kaj. 2014. Why Time Matters: Codon Evolution and the Temporal Dynamics of dN/dS. 31:212–231.

Navascues, M., and B.C. Emerson. 2009. Elevated substitution rate estimates from ancient DNA: model violation and bias of Bayesian methods. Mol. Ecol. 18:4390–4397.

Nielsen, R., and M.A. Beaumont. 2009. Statistical inferences in phylogeography. Mol. Ecol. 18:1034–1047.

Nuñez, J.J., N.K. Wood, F.E. Rabanal, F.M. Fontanella, and J.W. Jr. Sites. 2011. Amphibian phylogeography in the Antipodes: Refugia and postglacial colonization explain mitochondrial haplotype distribution in the Patagonian frog *Eupsophus calcaratus* (Cycloramphidae). Mol. Phyl. Evol. 58:343-352.

Ohta, T. 1973. Slightly deleterious mutant substitutions in evolution. Nature 246:96–98.

Olivieri, A., M. Pala, F. Gandini, B.H. Kashani, U.A. Perego, S.R. Woodward, V. Grugni, V. Battaglia, O. Semino, A. Achilli, M.B. Richards, and A. Torroni. (2013) Mitogenomes from Two Uncommon Haplogroups Mark Late Glacial/Postglacial Expansions from the Near East and Neolithic Dispersals within Europe. PLoS One 8:e70492.

Panova, M., A.M.H. Blakeslee, A.W. Miller, T. Maekinen, G.M. Ruiz, K. Johannesson, and C. Andre. 2011. Glacial History of the North Atlantic Marine Snail, *Littorina saxatilis*, Inferred from Distribution of Mitochondrial DNA Lineages. Plos One, 6: e17511.

Papadopoulou, A., I. Anastasiou, and A.P. Vogler. 2010. Revisiting the Insect Mitochondrial Molecular Clock: The Mid–Aegean Trench Calibration. Mol. Biol. Evol. 27:1659–1672.

Peter, B.M., D. Wegmann, and L. Excoffier. 2010. Distinguishing between population bottleneck and population subdivision by a Bayesian model choice procedure. Mol. Ecol. 19:4648–4660.

Peterson, G.I., and J. Masel. 2009. Quantitative Prediction of Molecular Clock and K–a/K–s at Short Timescales. Mol. Biol. Evol. 26:2595–2603.

Prost, S., R.P Guralnick, E. Waltari, V.B. Fedorov, E. Kuzmina, N. Smirnov, T. Van Kolfschoten, M. Hofreiter, and K. Vrieling. 2013. Losing ground: past history and future fate of Arctic small mammals in a changing climate. Glob. Change Biol. 19:1854–1864.

Provan, J., and K.D. Bennett. 2008. Phylogeographic insights into cryptic glacial refugia. Trends Ecol. Evol. 23:564–571.

Pybus, O.G., A. Rambaut, and P.H. Harvey. 2000. An integrated framework for the inference of viral population history from reconstructed genealogies. *Genetics* 155:1429–1437.

Rajabi–Maham, H., A. Orth, and F. Bonhomme. 2008. Phylogeography and postglacial expansion of *Mus musculus domesticus* inferred from mitochondrial DNA coalescent, from Iran to Europe. Mol. Ecol. 17:627–641.

Rambaut, A. 2000. Estimating the rate of molecular evolution: incorporating non-contemporaneous sequences into maximum likelihood phylogenies. Bioinformatics 16:395–399.

Rambaut, A., S.Y.W. Ho, A.J. Drummond, and B. Shapiro. 2009. Accommodating the Effect of Ancient DNA Damage on Inferences of Demographic Histories. Mol. Biol. Evol. 26:245–248.

Rannala, B. 1997. Gene genealogy in a population of variable size. Heredity 78:417–423.

Rambaut, A., M.A. Suchard, D. Xie, A.J. Drummond. 2013. Tracer v1.6, Available from http://beast.bio.ed.ac.uk/Tracer (accessed July 2014)

Raquin A.–L., F. Depaulis, A. Lambert, N. Galic, P. Brabant, and I. Goldringer. 2008. Experimental estimation of mutation rates in a wheat population with a gene genealogy approach. Genetics 179:2195–2211.

Rodriguez–Banderas, A., C.F. Vargas–Mendoza, A. Buonamici, and G.G. Vendramin. 2009. Genetic diversity and phylogeographic analysis of *Pinus leiophylla*: a post–glacial range expansion. J. Biogeogr. 36:1807–1820.

Ruzzante, D.E., S.J. Walde, J.C. Gosse, V.E. Cussac, E. Habit, T.S. Zemlak, and E.D. Adams. 2008. Climate control on ancestral population dynamics: insight from Patagonian fish phylogeography. Mol. Ecol. 17:2234–2244.

Shapiro, B., A.J. Drummond, A. Rambaut, M.C. Wilson, P.E. Matheus, A.V. Sher, O.G. Pybus, M.T.P. Gilbert, I. Barnes, J. Binladen, E. Willerslev, A.J. Hansen, G.F.

Baryshnikov, J.A. Burns, S. Davydov, J.C. Driver, D.G. Froese, C.R. Harington, G. Keddie, P. Kosintsev, M.L. Kunz, L.D. Martin, R.O. Stephenson, J. Storer, R. Tedford, S. Zimov, and A. Cooper. 2004. Rise and fall of the Beringian steppe bison. Science 306:1561–1565.

Shields, G.F., and A.C. Wilson. 1987. Calibration of mitochondrial–DNA evolution in geese. J. Mol. Evol. 24:212–217.

Small, M.P., and E.M. Gosling. 2000. Genetic structure and relationships in the snail species complex *Littorina arcana* hannaford ellis, *L. compressa* Jeffreys and *L. saxatilis* (Olivi) in the British isles using SSCPs of cytochrome-b fragments. Heredity 84:692–701

Soares, P., L. Ermini, N. Thomson, M. Mormina, T. Rito, A. Rohl, A. Salas, S. Oppenheimer, V. Macaulay, and M.B. Richards. 2009. Correcting for Purifying Selection: An Improved Human Mitochondrial Molecular Clock. Am. J. Hum. Genet. 84:740–759.

Städler, T., B. Haubold, C. Merino, W. Stephan, and P. Pfaffelhuber. 2009. The Impact of Sampling Schemes on the Site Frequency Spectrum in Nonequilibrium Subdivided Populations. Genetics 182:205–216.

Subramanian, S. 2009. Temporal Trails of Natural Selection in Human Mitogenomes. Mol. Biol. Evol. 26:715–717.

Subramanian, S., and D.M. Lambert. 2011. Time Dependency of Molecular Evolutionary Rates? Yes and No. Genome Biol. Evol. 3:1324–1328.

Suchard, M.A., R.E. Weiss, and J.S. Sinsheimer. 2001. Bayesian selection of continuous–time Markov chain evolutionary models. Mol. Biol. Evol. 18:1001–1013.

Sullivan, J. and P. Joyce. 2005. Model selection in phylogenetics. Ann. Rev. Ecol. Syst. 36:445–466.

Tamura, K., D. Peterson, N. Peterson, G. Stecher, M. Nei, and S. Kumar. 2011. MEGA5: Molecular Evolutionary Genetics Analysis Using Maximum Likelihood, Evolutionary Distance, and Maximum Parsimony Methods. Mol. Biol. Evol. 28:2731–2739.

Wakeley, J. 1999. Nonequilibrium migration in human history. Genetics 153:1863–1871.

Walker, M., S. Johnsen, S.O. Rasmussen, T. Popp, J.-P. Steffensen, P. Gibbard, W. Hoek, J. Lowe, J. Andrews, S. Björck, L.C. Cwynar, K. Hughen, P. Kershaw, B. Kromer, T. Litt, D.J. Lowe, T. Nakagawa, R. Newnham, and J. Schwander. 2009. Formal definition and dating of the GSSP (Global Stratotype Section and Point) for the base of the Holocene using the Greenland NGRIP ice core, and selected auxiliary records. J. Quaternary Sci. 24:3–17.

Williams, M.A.J., S.H. Ambrose, S. van der Kaars, C. Ruehlemann, U. Chattopadhyaya, J. Pal, and P.R. Chauhan. 2009. Environmental impact of the 73 ka Toba super-eruption in South Asia. Palaeogeogr. Palaeoclimatol. Palaeoecol. 284:295–314.

Wu, C.I., and W.H. Li. 1985. Evidence for higher rates of nucleotide substitution in rodents than in man. Proc. Natl. Acad. Sci. U.S.A. 82:1741–1745.

Zhivotovsky L.A., P.A. Underhill, C. Cinnioğlu, M. Kayser, B. Morar, T. Kivisild, R. Scozzari, F. Cruciani, G. Destro-Bisol, G. Spedini, G.K. Chambers, R.J. Herrera, K.K. Yong, D. Gresham, I. Tournev, M.W. Feldman, and L. Kalaydjieva. 2004. The effective mutation rate at Y chromosome short tandem repeats, with application to human population–divergence time. Am. J. Hum. Genet. 74:50–61.

Zuckerkandl, E., and L. Pauling. 1962. Molecular disease, evolution, and genic heterogeneity. *Horizons in Biochemistry*, eds Kasha M, Pullman B (Academic Press, New York), pp 189–225.

# Appendix

## Appendix 1: Details of Empirical data Sets

### *Rough Periwinkle* Littorina saxatilis

Main reference: Doellman et al. (2011) and Panova et al. (2011).

Data set: Sequences of the species found on GenBank.

Taxon distribution and habitats: Intertidal bedrocks of the North-West Atlantic Ocean.

GenBank identifier: AF146647.1; AJ237709.1-AJ237715.1; EF114083.1-EF114095.1; EF114097.1-EF114101.1; JF340294.1-JF340318.1; JF340320.1-JF340366.1; JF501842.1-JF501843.1; JF501860.1-JF501952.1; U46817.1.

### *Palearctic Bark Beetle* Pityogenes chalcographus

Main reference: Bertheau et al. (2013).

Data set: Whole species.

Taxon distribution and habitats: Widespread in continental Europe and concordant with the distribution of its host, the Norway spruce *Picea abies*.

GenBank identifier: KC514357-KC514450.

### *Chocolate Chip Starfish* Protoreaster nodosus

Main reference: Crandall et al. (2012).

Data set: West Pacific lineage.

Taxon distribution and habitats: Coral reefs and seagrasses of the Indo-West Pacific region.

GenBank identifier: FJ386008.1-FJ386094.1.

### *Three-Spined Stickleback* Gasterosteus aculeatus

Main reference: Mäkinen and Merilä (2008).

Data set: European lineage.

Taxon distribution and habitats: Coastal waters or freshwater bodies of the North-East Atlantic Ocean.

GenBank identifier: EF525391.1-EF525476.1.

### *Patagonian Frog* Eupsophus calcaratus

Main reference: Nuñez et al. (2011).

Data set: Lineage F.

Taxon distribution and habitats: Subantarctic forests, rivers, swamps, and marshes in Argentina and Chile.

GenBank identifier: HQ710840.1-HQ710847.1; HQ710849.1-HQ710927.1.

***European Brown Bear* Ursus arctos**

Main reference: Korsten et al. (2009).

Data set: Lineage 3a.

Taxon distribution and habitats: Broad range of habitats in Eurasia.

GenBank identifier: EU526765.2-EU526814.2.

***European Human* Homo sapiens sapiens**

Main reference: Li et al. (2014).

Data set: Lineage Haplogroup H1, 100 sequences randomly selected from an original set of 340 sequences.

Taxon distribution and habitats: Danish.

GenBank identifier: KF161085.1; KF161123.1; KF161129.1; KF161142.1; KF161145.1; KF161188.1; KF161192.1; KF161197.1; KF161250.1; KF161255.1; KF161259.1; KF161266.1; KF161267.1; KF161271.1; KF161304.1; KF161352.1; KF161354.1; KF161372.1; KF161374.1; KF161395.1; KF161448.1; KF161458.1; KF161470.1; KF161478.1; KF161480.1; KF161485.1; KF161503.1; KF161536.1; KF161548.1; KF161551.1; KF161588.1; KF161598.1; KF161613.1; KF161639.1; KF161642.1; KF161648.1; KF161655.1; KF161681.1; KF161726.1; KF161760.1; KF161765.1; KF161771.1; KF161784.1; KF161850.1; KF161859.1; KF161865.1; KF161873.1; KF161888.1; KF161892.1; KF161899.1; KF161926.1; KF161931.1; KF161942.1; KF161962.1; KF161991.1; KF162004.1; KF162011.1; KF162014.1; KF162037.1; KF162041.1; KF162079.1; KF162082.1; KF162086.1; KF162095.1; KF162109.1; KF162111.1; KF162136.1; KF162189.1; KF162200.1; KF162216.1; KF162236.1; KF162246.1; KF162287.1; KF162324.1; KF162343.1; KF162348.1; KF162358.1; KF162401.1; KF162418.1; KF162442.1; KF162482.1; KF162498.1; KF162511.1; KF162516.1; KF162522.1; KF162599.1; KF162614.1; KF162631.1; KF162634.1; KF162709.1; KF162765.1; KF162859.1; KF162883.1; KF162909.1; KF162910.1; KF162913.1; KF162945.1; KF162954.1; KF163017.1; KF163046.1.

## Appendix 2: Estimates of Divergence Rates

### Calibration Based on the Closure of the Central American Isthmus for Starfish and Periwinkle

For the divergence rate of the starfish, no good fossil record exists, so I used the rate available for echinoids obtained by calibrating the vicariance that happened after the closure of the Central American Isthmus based on the COI. I used the clock available for echinoids by averaging the values obtained for the eight species of echinoids (table 1 in Lessios 2008) that show a split at the end of the closure of the Isthmus at 2.8 Ma. The rate obtained was 0.0191 changes/site/myr (95% confidence interval, CI: 0.0126–0.0257) with a standard deviation of 0.0033. For the periwinkle, the same approach was used to obtain the divergence rate for the cyt *b*

. Because no cyt *b*

data are available yet to calibrate this vicariance, I used the rates derived using the COI for Gastropoda. The rate was obtained from four species (table 4 in Lessios 2008) and was 0.0146 (CI: 0.0116–0.0177) changes/site/myr with a standard deviation of 0.0015.

### Calibration for Bark Beetles

To calibrate the genealogies of bark beetles, Bertheau et al. (2013) used the average of three divergence rates (0.0187) based on fossils, biogeography, and geology (0.5–29.0 Ma) and obtained for COI in Coleoptera (Borer et al. 2010). I recovered these divergence rates and obtained a per lineage rate of 0.0093 changes/site/myr with a standard deviation of 0.0028.

### Fossil Calibration for Sticklebacks

I used a fossil dating back to 10 Ma (Small and Gosling 2000; Mäkinen and Merilä 2008) with 1 myr standard deviation as a calibration between the three-spined stickleback (*Gasterosteus aculeatus*; $N$=22

) and nine-spined stickleback (*Pungitius pungitius*; $N$=21). So, it is the dating of the *TMRCA* for the two species based on 971 bp of cytochrome *b*. Samples of *Gasterosteus aculeatus* (AB094606.1–AB094627.1) and *Pungitius pungitius* (GU227740.1, GU227742.1, GU227762.1, GU227782.1, GU227783.1, JF798873.1, JF798874.1, JF798900.1, JF798901.1, JF798914.1, JF798915.1, JF798928.1, JF798929.1, JQ983013.1, JQ983014.1, JQ983040.1, JQ983041.1, JQ983061.1, JQ983062.1, JQ983069.1, JQ983070.1). The mean phylogenetic rate obtained was 0.0191 changes/site/myr with a 95% posterior probability (HPD) of 0.0081–0.0332 and a standard deviation of 0.0082. This value is fairly close to what Mäkinen and Merilä (2008) found in their study (0.0205), but the new estimate has the advantage of providing levels of uncertainty around the mean molecular rate.

### Anurans Substitution Rate for Frogs

To calibrate the clock on Patagonian frog, Nuñez et al. (2011) used the rates calculated by Crawford (2003) on anurans. The latter calculated substitution rates for the ND2 between 0.0148 and 0.0245 changes/site/myr among different groups. The rates were based on three lineages of frogs (Anura: Leptodactylidae) belonging to the genus *Eleutherodactylus* and the subgenus *Craugastor* occurring in Central America. From these two values, I derived the average and standard deviation for the lineage rate ($0.0098 \pm 0.0034$ changes/site/myr), which I then used as a divergence rate.

### Calibration Based on the Common Ancestor between Brown and Black Bears

A previous paper used mitogenomic data to assess the phylogenetic relationships between the polar bear *Ursus maritimus*, the brown bear *Ursus arctos*, and the American black bear *Ursus americanus* (Krause et al. 2008). They found a very complex relationship but identified a common ancestor between the brown bear and the black bear dating from 4 to 5 Ma. I used these assumptions to estimate the molecular rate for the control region using available sequences of both brown (HQ685905.1, HQ685914.1, HQ685919.1, HQ685924.1, HQ685931.1, HQ685935.1, HQ685941.1, HQ685947.1, HQ685954.1, HQ685961.1, NC003427.1) and black bear (AF303109.1, JX196366.1, NC003426.1) on GenBank. The estimated rate from this calibration was 0.0128 changes/site/myr (HPD: 0.0076–0.0200) with a standard deviation around 0.0041.

### Calibration Based on the Common Ancestor of Homo-Pan for Human

I used the assumptions of a 6.5 Ma (0.65 for standard deviation) common ancestor between Human and Chimpanzee (Soares et al. 2009) to calibrate the control region obtained from the Human haplogroup H1 (KJ486160.1, KF466257.1, HQ659703.1, KC911565.1, KF429262.1, EF093539.1, EF093536.1, EF093535.1, EF093538.1, EF093537.1, AY195783.2, AF347008.1, AF347009.1, AY195780.1, AY195789.2) and the two species of Chimpanzee (JF727202.2, JF727205.1, JF727204.1, JF727203.1, JN191233.1, HM015213.1, GU189677.1, GU189676.1, GU189674.1, GU189673.1). The rate estimate from this calibration was $0.0280 \pm 0.0077$ (HPD: 0.0166–0.0464) changes/site/myr.